Anal. Chem. **2010,** *82,* 6104–6114

Accurate Spectroscopic Calibration for Noninvasive Glucose Monitoring by Modeling the Physiological Glucose Dynamics

Ishan Barman,* Chae-Ryon Kong, Gajendra P. Singh,† Ramachandra R. Dasari, and Michael S. Feld‡

G. R. Harrison Spectroscopy Laboratory, Massachusetts Institute of Technology, Cambridge, Massachusetts 02139

The physiological lag between blood and interstitial fluid (ISF) glucose is a major challenge for noninvasive glucose concentration measurements. This is a particular problem for spectroscopic techniques, which predominantly probe ISF glucose, creating inconsistencies in calibration, where blood glucose measurements are used as a reference. To overcome this problem, we present a dynamic concentration correction (DCC) scheme, based on the mass transfer of glucose between blood and ISF, to ensure consistency with the spectral measurements. The proposed formalism allows the transformation of glucose in the concentration domain, ensuring consistency with the acquired spectra in the calibration model. Taking Raman spectroscopy as a specific example, we demonstrate that the predicted glucose concentrations using the DCC-based calibration model closely match the measured glucose concentrations, while those generated with the conventional calibration methods show significantly larger deviations from the measured values. In addition, we provide an analytical formula for a previously unidentified source of limiting uncertainty arising in spectroscopic glucose monitoring from a lack of knowledge of glucose kinetics in prediction samples. A study with human volunteers undergoing glucose tolerance tests indicates that this lag uncertainty, which is comparable in magnitude to the uncertainty arising from noise and nonorthogonality in the spectral data set, can be reduced substantially by employing the DCC scheme in spectroscopic calibration.

Noninvasive glucose diagnosis has received considerable attention due to its important implications for diabetes management and therapeutics.[1,2] Various techniques ranging from electrochemical assays[3,4] to optical methods[5] have been proposed to meet the goals of painless and accurate glucose measurements. Vibrational spectroscopy, notably near-infrared (NIR) absorption and Raman spectroscopy, has shown substantial promise in this regard.[6] Specifically, NIR−Raman spectroscopy has provided successful predictions of glucose at physiologically relevant concentrations in serum,[7,8] whole blood,[9] and even human volunteers.[10] However, a clinically accurate and robust algorithm for predicting glucose concentrations in multiple human subjects, or even in the same subject at different times, is currently lacking.[11]

Researchers have identified factors that degrade the glucose measurement accuracy of Raman spectroscopy by introducing non-analyte-specific variance into the calibration model. The predominant factors include sample-to-sample variability in absorption and scattering properties (turbidity),[12] tissue autofluorescence and associated quenching,[13] and physiological lag between blood and interstitial fluid (ISF) glucose.[14−18] Several spectroscopic correction schemes have been implemented to minimize the effect of the first two factors,[19−21] but correction for the presence of a lag time has not been demonstrated for transcutaneous glucose monitoring, due to its intricate relationship with the fundamental physiological dynamics. This lag time creates an inconsistency in spectroscopic calibration algorithms, which are based on reference blood glucose concentrations and the acquired tissue spectra. This inconsistency arises from the fact that the spectro-

* To whom correspondence should be addressed. E-mail: ishan@mit.edu.

† Current address: School of Physics and Astronomy, University of St. Andrews, St. Andrews KY16 9SS, Scotland.

‡ Deceased.

(1) Khalil, O. S. *Clin. Chem.* **1999**, *45*, 165–177.
(2) Khalil, O. S. *Diabetes Technol. Ther.* **2004**, *6*, 660–697.
(3) Heller, A. *Annu. Rev. Biomed. Eng.* **1999**, *1*, 153–175.
(4) Tierney, M. J.; Tamada, J. A.; Potts, R. O.; Jovanovic, L.; Garg, S. *Biosens. Bioelectron.* **2001**, *16*, 621–629.
(5) Tuchin, V. V. *Tissue Optics: Light Scattering Methods and Instruments for Medical Diagnosis*; SPIE (Society of Photo-optical Instrumentation Engineers) Press: Bellingham, WA, 2000.
(6) Arnold, M. A.; Small, G. W. *Anal. Chem.* **2005**, *77*, 5429–5439.
(7) Qu, J. N. Y.; Wilson, B. C.; Suria, D. *Appl. Opt.* **1999**, *38*, 5491–5498.
(8) Rohleder, D.; Kiefer, W.; Petrich, W. *Analyst* **2004**, *129*, 906–911.
(9) Enejder, A. M. K.; Koo, T. W.; Oh, J.; Hunter, M.; Sasic, S.; Feld, M. S.; Horowitz, G. L. *Opt. Lett.* **2002**, *27*, 2004–2006.
(10) Chaiken, J.; Finney, W.; Knudson, P. E.; Weinstock, R. S.; Khan, M.; Bussjager, R. J.; Hagrman, D.; Hagrman, P.; Zhao, Y. W.; Peterson, C. M.; Peterson, K. *J. Biomed. Opt.* **2005**, *10*, 031111.
(11) Enejder, A. M. K.; Scecina, T. G.; Oh, J.; Hunter, M.; Shih, W.-C.; Sasic, S.; Horowitz, G.; Feld, M. S. *J. Biomed. Opt.* **2005**, *10*, 031114.
(12) Aarnoutse, P. J.; Westerhuis, J. A. *Anal. Chem.* **2005**, *77*, 1228–1236.
(13) Zeng, H.; MacAulay, C.; McLean, D. I.; Palcic, B.; Lui, H. *Photochem. Photobiol.* **1998**, *68*, 227–236.
(14) Boyne, M. S.; Silver, D. M.; Kaplan, J.; Saudek, C. D. *Diabetes* **2003**, *52*, 2790–2794.
(15) Cengiz, E.; Tamborlane, W. V. *Diabetes Technol. Ther.* **2009**, *11*, S-11–16.
(16) Kulcu, E.; Tamada, J. A.; Reach, G.; Potts, R. O.; Lesho, M. J. *Diabetes Care* **2003**, *26*, 2405–2409.
(17) Rebrin, K.; Steil, G. M. *Diabetes Technol. Ther.* **2000**, *2*, 461–472.
(18) Thennadil, S. N.; Rennert, J. L.; Wenzel, B. J.; Hazen, K. H.; Ruchti, T. L.; Block, M. B. *Diabetes Technol. Ther.* **2001**, *3*, 357–365.
(19) Barman, I.; Singh, G. P.; Dasari, R. R.; Feld, M. S. *Anal. Chem.* **2009**, *81*, 4233–4240.
(20) Matousek, P.; Towrie, M.; Stanley, A.; Parker, A. W. *Appl. Spectrosc.* **1999**, *53*, 1485–1489.
(21) Lieber, C. A.; Mahadevan-Jansen, A. *Appl. Spectrosc.* **2003**, *57*, 1363–1367.

10.1021/ac100810e
Published on Web 06/24/2010

scopic techniques primarily probe ISF glucose,[18] due to the relatively shallow penetration depth (~1 mm) of NIR light in tissue and the small density of blood vessels in the superficial layers of the skin.[22]

This inconsistency in calibration presents a severe hindrance not only for spectroscopy-based noninvasive glucose monitoring but also for minimally invasive electrochemical sensors (such as Medtronic/Minimed's Guardian and FreeStyle Navigator from Abbott Diabetes Care), which base their glucose estimates on interstitial fluid measurements. Indeed, as pointed out by Cengiz and Tamborlane,[15] the physiological lag introduces systematic errors during calibration which adversely impact long-term sensor performance, even in the presence of a positive correlation between blood and ISF glucose.[23−25] Such diagnostic errors may lead to unnecessary insulin bolus, which significantly increases the risk of hypoglycemia.[26,27] The presence of systematic errors is one of the main reasons that such continuous glucose monitoring sensors need to be recalibrated against fingerstick measurements at regular intervals.

Typically, for all ISF glucose-based sensors, spectroscopic or otherwise, the underlying assumption is that the blood-to-ISF glucose gradient remains constant over the measurement range.[17] However, this assumption fails if the sensor is calibrated during rapid changes in blood glucose, as are encountered during glucose tolerance tests, which provide the most viable protocol for the development of calibration models using spectroscopic techniques.[28] Calibration during such nonequilibrium conditions leads to large errors in the developed model. To account for the differences in blood and ISF glucose, Bonnecaze and co-workers established the first substantive models for ISF glucose by considering the ISF and blood glucose to reside in two "compartments" and performing a mass balance between them.[29,30] Using amperometric glucose sensors implanted in rats, they demonstrated that accurate estimates of blood glucose concentration can be extracted from subcutaneous ISF glucose-based measurements. However, no analogous models exist for development of spectroscopic calibration algorithms, which are inherently more complex because of the multivariate nature of the data.

Furthermore, even if an accurate calibration model can be established by performing all measurements under equilibrium conditions (e.g., by employing glucose clamps), the lack of knowledge of glucose kinetics in prediction samples would introduce an uncertainty in the concentration estimates. Such prediction uncertainties may lead to inappropriate treatments. Previously, several research groups have assessed uncertainty in spectroscopic prediction based on the noise in the spectral and concentration data sets and the nonorthogonality (spectral overlap) of the analyte of interest with the other sample constituents.[31−33] However, the uncertainty introduced due to the lag phenomenon in the prediction samples remains unexplored.

In this paper we present a new spectroscopic calibration scheme based on a "dynamic concentration correction" (DCC), which is based on a two-compartment mass transfer picture of blood and ISF glucose and is designed to provide an accurate estimate of glucose concentrations for noninvasive measurements. These transformations are performed iteratively in conjunction with an implicit calibration method, such as partial least-squares (PLS), to form an accurate and consistent regression model. The resulting calibration model can be used on a new set of acquired spectral samples—the prediction set—to calculate the ISF glucose concentrations of the samples. Subsequent application of the DCC model converts the estimated ISF glucose concentrations to the equivalent blood glucose concentrations of the prediction samples.

This work employs Raman spectroscopy as a specific example to demonstrate the effectiveness of the new calibration method, with the understanding that this scheme can be similarly applied to other spectroscopic techniques, such as NIR absorption. Using blood and ISF glucose concentration data sets obtained by Steil et al.,[34] we first demonstrate that predicted glucose concentrations using the DCC calibration model closely match the measured blood glucose concentrations, whereas those generated solely by the conventional implicit calibration methods show significantly larger deviations from the measured values. These results are further validated on spectral and concentration data sets obtained from clinical studies on human volunteers undergoing glucose tolerance tests.

In addition, we derive analytical expressions for the limiting uncertainty introduced into the concentration predictions due to the presence of the physiological lag—with and without application of the DCC. Here, limiting uncertainty is defined as the uncertainty in the concentration estimate in the case where all modeling noise is disregarded, i.e., where the calibration model is assumed to be completely accurate and noise free. Employing the human volunteer data, we find that the concentration uncertainty due to the lag phenomenon is comparable to that arising from the noise and overlap in the prediction spectra and that this major source of uncertainty can be significantly reduced (approximately 6-fold) when the DCC is used, providing further motivation for its use in spectroscopy-based transcutaneous blood glucose monitoring.

DYNAMIC CONCENTRATION CORRECTION THEORY

The primary motivation for proposing a new spectroscopic calibration method for blood glucose detection is to establish consistency in the calibration model, which maps the spectral measurements to the glucose concentrations. The conventional linear calibration equation can be written as[35]

$$\mathbf{b} = \mathbf{S}^{*}\mathbf{c} \tag{1}$$

(22) McGrath, J. A.; Eady, R. A.; Pope, F. M. *Rook's Textbook of Dermatology*; Blackwell Publishing: Malden, MA, 2004.
(23) Bolinder, J.; Ungerstedt, U.; Arner, P. *Diabetologia* **1992**, *35*, 1177–1180.
(24) Reach, G.; Wilson, G. S. *Anal. Chem.* **1992**, *64*, 381A–386A.
(25) Lonnroth, P.; Jansson, P. A.; Smith, U. *Am. J. Physiol.* **1987**, *253*, E228–E231.
(26) The Diabetes Control and Complications Trial Research Group. *N. Engl. J. Med.* **1993**, *329*, 977−986.
(27) The Diabetes Control and Complications Trial Research Group. *Diabetes Care* **1995**, *18*, 1415−1427.
(28) Heise, H. M.; Marbach, R.; Koschinsky, T. H.; Gries, F. A. *Artif. Organs* **1994**, *18*, 439–447.
(29) Schmidtke, D. W.; Freeland, A. C.; Heller, A.; Bonnecaze, R. T. *Proc. Natl. Acad. Sci. U.S.A.* **1998**, *95*, 294–299.
(30) Freeland, A. C.; Bonnecaze, R. T. *Ann. Biomed. Eng.* **1999**, *27*, 525–537.
(31) Lorber, A.; Kowalski, B. *J. Chemom.* **1988**, *2*, 93–109.
(32) Berger, A. J.; Feld, M. S. *Appl. Spectrosc.* **1997**, *51*, 725–732.
(33) Ścepanovic, O. R.; Bechtel, K. L.; Haka, A. S.; Shih, W. C.; Koo, T. W.; Berger, A. J.; Feld, M. S. *J. Biomed. Opt.* **2007**, *12*, 064012.
(34) Steil, G. M.; Rebrin, K.; Hariri, F.; Jinagonda, S.; Tadros, S.; Darwin, C.; Saad, M. F. *Diabetologia* **2005**, *48*, 1833–1840.
(35) Brereton, R. G. *Applied Chemometrics for Scientists*; John Wiley & Sons Ltd.: Chichester, West Sussex, England, 2007.

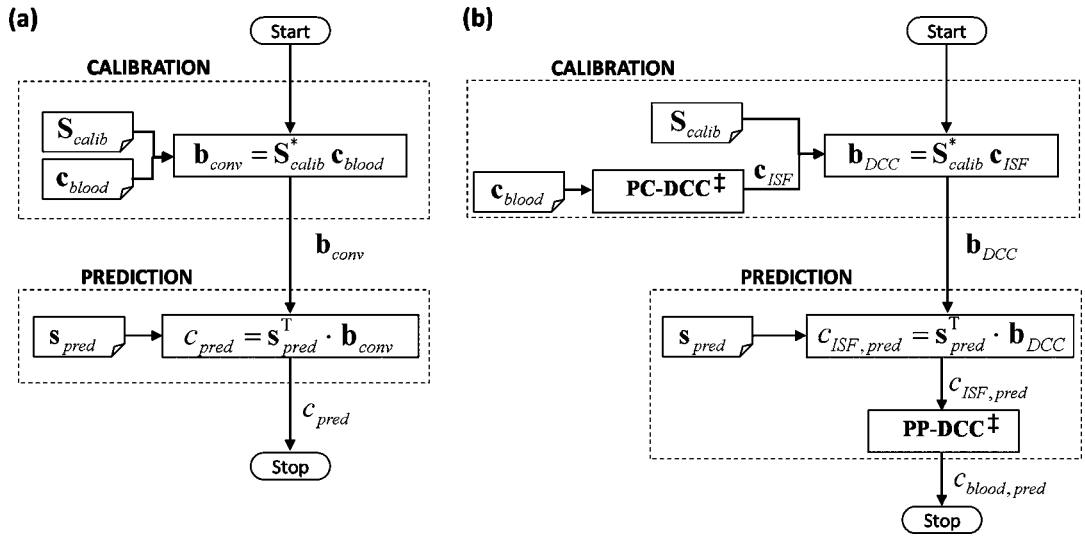

Figure 1. Flowcharts of the (a) conventional implicit and (b) DCC calibration methods. $\mathbf{S}_{calib}$, $\mathbf{c}_{blood}$, and $\mathbf{s}_{pred}$ represent the calibration spectra, reference blood glucose concentrations in the calibration samples, and spectrum acquired from the prediction sample, respectively. For the conventional calibration method, $\mathbf{b}_{conv}$ and c_{pred} give the regression vector and the predicted concentration, respectively. For DCC calibration, $\mathbf{b}_{DCC}$ represents the developed regression vector. $c_{ISF,pred}$ and $c_{blood,pred}$ are the intermediate ISF glucose estimate and the final blood glucose prediction. PC-DCC is the precalibration transformation of blood glucose concentrations into the corresponding ISF glucose values. PP-DCC transforms the predicted ISF glucose concentration into the blood glucose value. Note that the conventional calibration scheme does not differentiate between the blood and ISF glucose concentrations. Note (see ‡ symbol): Both PP-DCC and PC-DCC require two concentration inputs acquired at a time interval Δt apart for evaluation of eqs 15 and 16b, respectively.

where **b** is the spectrum of regression coefficients (also called the regression vector), **S** is the matrix of calibration spectra, and **c** is the vector of measured concentrations of the analyte of interest in the calibration samples. **S*** is the appropriate inverse of **S**, as evaluated by the calibration method of choice. (A lowercase boldface letter represents a vector, and an uppercase boldface letter denotes a matrix.)

As mentioned in the introduction, since the spectral measurements are predominantly contributed by ISF glucose, the relevant input concentrations to the implicit calibration method should incorporate the ISF glucose concentrations. However, the ISF glucose concentrations are typically not available in a real-life clinical setting; instead, blood glucose values obtained from frequent blood withdrawals are used as reference concentrations. This creates a regression vector, which is based neither completely on blood glucose nor completely on ISF glucose, but a mixture of the two contributions. This, in turn, also creates a problem in the prediction step, where the predicted glucose concentration, c, is obtained by a scalar product of the regression vector, **b**, and the spectrum acquired from the prediction sample, **s**:

$$c = \mathbf{s}^{\mathrm{T}} \cdot \mathbf{b} \tag{2}$$

(A lowercase italic letter indicates a scalar quantity, and the superscript "T" denotes the transpose of the vector.) In the conventional calibration framework, the predicted glucose concentration is reported as the blood glucose concentration, although this clearly is not an accurate representation.

To correct for this discrepancy, we propose a new calibration methodology (DCC) in which the concentrations are appropriately changed to conform to the spectral measurements. The transformation in the concentration domain is based on a two-compartment mass transfer model, which establishes a well-defined relationship between blood glucose, ISF glucose, and the system parameters. Specifically, we perform the following two transformations in DCC. (a) Precalibration DCC (PC-DCC): Transform the blood glucose concentrations in the calibration data set to their corresponding ISF values before inputting them into the implicit calibration method. This ensures that the regression vector is solely based on ISF glucose contributions. (b) Postprediction DCC (PP-DCC): Retransform the predicted ISF glucose concentration, which is determined by eq 2, to the corresponding blood glucose value. The conceptual differences between the conventional and proposed (DCC-based) calibration methods can be seen in Figure 1.

For the subsequent analysis, we assume that the sampling volume (i.e., the volume of tissue probed by the NIR light) is a subset of the interstitial fluid space. This assumption is primarily based on the fact that the ISF constitutes nearly 45% of the volume fraction of the human skin in contrast to the blood vessels, which contribute about 5% of the skin volume.[36] In the Results and Discussion, we revisit this assumption and characterize its impact on the proposed calibration model.

Transfer of glucose from the blood to the ISF compartment occurs by passive diffusion across an established concentration gradient.[37] The mass transfer rate is affected by several variables, such as the blood flow rate to the site, rate of glucose uptake by the surrounding tissue, and capillary permeability. Nevertheless, as discussed in the literature,[29,34,38] a simple two-compartment mass transfer model can be written for the ISF volume, V_{ISF}:

$$V_{\mathrm{ISF}}\frac{\mathrm{d}c_{\mathrm{ISF}}}{\mathrm{d}t} = k_{\mathrm{M}}A(c_{\mathrm{BG}} - c_{\mathrm{ISF}}) - k_{\mathrm{U}}V_{\mathrm{ISF}}c_{\mathrm{ISF}} \tag{3}$$

(36) Roe, J. N.; Smoller, B. R. *Crit. Rev. Ther. Drug Carrier Syst.* **1998**, *15*, 199–241.
(37) Zierler, K. *Am. J. Physiol.* **1999**, *276*, E409–E426.
(38) Rebrin, K.; Steil, G. M.; van Antwerp, W. P.; Mastrototaro, J. J. *Am. J. Physiol.* **1999**, *277*, E561–E571.

where c_{ISF} and c_{BG} are the ISF and blood glucose concentrations (mol/cm^3), respectively, k_M is the glucose mass transfer coefficient (cm/s), A is the effective mass transfer surface area (cm^2), and k_U is the rate of glucose uptake by the neighboring cells (s^{-1}). The effect of insulin on the uptake term has been ignored. This approximation is consistent with the observed result that the glucose levels in (subcutaneous) ISF are largely unaffected by the local insulin concentration.[34] In fact, the uptake term itself has been observed to be very small for subcutaneous glucose sensing.[29] This is attributed to the fact that skin tissue, as opposed to muscle or adipose tissue, is unlikely to have significant glucose uptake, even in the presence of a high insulin concentration. Consequently, we will ignore the uptake term in further analysis. Equation 3 can then be simplified to

$$c_{BG} = c_{ISF} + \alpha \frac{dc_{ISF}}{dt} \quad (4)$$

where α ($=V_{ISF}/k_M A$) is a lumped mass transfer parameter having units of time. The parameter α provides a measure of the physiological lag time arising from the diffusion process and is henceforth called the characteristic lag time constant. This equation provides the ability to construct blood glucose estimates based on the spectroscopy-based ISF glucose prediction values and a priori knowledge of the lag time constant in the sample. The numerical evaluation of this equation, which provides the postprediction (PP-DCC) step, is explained in Appendix I.

The other important portion of the proposed scheme is the precalibration (PC-DCC) step. To obtain consistency in the calibration model, we need to convert the measured blood glucose concentrations to the corresponding ISF glucose values. To perform this transformation, we write eq 4 in its integral form:

$$c_{ISF}(t_f) = c_{ISF}(t_i) \exp\left(-\frac{1}{\alpha}(t_f - t_i)\right) + \frac{1}{\alpha}\int_{t_i}^{t_f} c_{BG} \times \exp\left(-\frac{1}{\alpha}(t_f - t_i)\right) dt \quad (5)$$

where the definite integral is evaluated from time t_i to time t_f. Details of the numerical implementation of this equation are given in Appendix II.

FORMULATION OF PREDICTION UNCERTAINTY ARISING FROM PHYSIOLOGICAL LAG

To quantify the precision of spectroscopy-based calibration models, Lorber and Kowalski derived an elegant prediction error formula, which describes the error propagation for linear multivariate prediction algorithms.[31] Our laboratory has previously derived analytical expressions for uncertainty in concentration prediction for the specific case where noise in the prediction data set (spectra) is the dominant source of error.[32,33] This case is important, as in most biomedical applications constraints on the acquisition time in prediction samples cause the noise in the prediction data set to be significantly higher than that observed in the calibration data set (where acquisition times are typically much longer). In such cases, it can be assumed that an accurate calibration model can be achieved by developing it on calibration samples in which a sufficiently high signal-to-noise ratio (SNR) can be attained. Under such conditions, the limiting uncertainty in the predicted concentrations arises from the spectral overlap between the analyte of interest and the other tissue constituents and the measurement noise in the spectra acquired from the prediction samples. Mathematically, the spectroscopic uncertainty for the analyte of interest (glucose) is given by Δc_s:[33]

$$\hat{c} = (\mathbf{s} \pm \Delta\mathbf{s})^T \cdot \mathbf{b} = \mathbf{s}^T \cdot \mathbf{b} \pm \Delta\mathbf{s}^T \cdot \mathbf{b} = c \pm \Delta c_s \quad (6a)$$

where

$$\Delta c_s = \frac{\sigma}{s_g}(\text{olf}) \quad (6b)$$

Here, $\hat{c}$ and c are the estimated and actual analyte concentrations in the prediction sample, respectively, and $\Delta\mathbf{s}$ represents the spectral noise in the prediction spectrum, $\mathbf{s}$. As the modeling noise is ignored in computation of the limiting uncertainty, $\mathbf{b}$ represents the ideal (noise-free) regression vector for glucose. σ is a measure of the noise magnitude in the prediction spectrum, s_g quantifies the signal strength of glucose at unit concentration, and olf indicates the amount of overlap between glucose and the other spectral interfering agents (such as proteins, lipids, and water).

In addition to the spectroscopic uncertainty, there exists a prediction uncertainty for transcutaneous glucose measurements that arises from the physiological lag between blood and ISF glucose levels. Even if the calibration models are developed under conditions in which the blood and ISF glucose concentrations are in equilibrium (such as those obtained by employing glucose/insulin clamps), the predicted concentrations will still contain uncertainties due to the unaccounted physiological lag in the prediction samples. We present an error propagation analysis to determine the limiting uncertainty in concentration prediction due to the physiological lag, with and without DCC. Similar to our laboratory's previous work,[32,33] we assume that the developed calibration model itself is accurate, i.e., devoid of noise and lag-related errors.

Limiting Uncertainty for Conventional Calibration. When the modeling noise is ignored, eq 6a provides the relationship between the estimated and the actual glucose concentrations. However, for in vivo prediction, there will be a lag between the instantaneous blood and ISF glucose values in the sample, where the latter is measured by the prediction spectrum. Taking this into account, we can rewrite eq 6b in terms of the estimated ($\hat{c}_{ISF}$) and actual (c_{ISF}) ISF glucose concentrations:

$$\hat{c}_{ISF} = (\mathbf{s} \pm \Delta\mathbf{s})^T \cdot \mathbf{b} = c_{ISF} \pm \Delta c_s \quad (7)$$

On the basis of the two-compartment model, the actual blood glucose concentration, c_{BG}, can be determined from the actual ISF glucose concentration using eq 4, given the correct lag time constant for the prediction sample (α_{actual}). Substituting the value of the actual ISF glucose concentration from eq 7 into eq 4, we obtain

$$c_{BG} = c_{ISF} + \alpha_{actual}\frac{dc_{ISF}}{dt} = \hat{c}_{ISF} + \alpha_{actual}\frac{d\hat{c}_{ISF}}{dt} \pm \Delta c_s \quad (8)$$

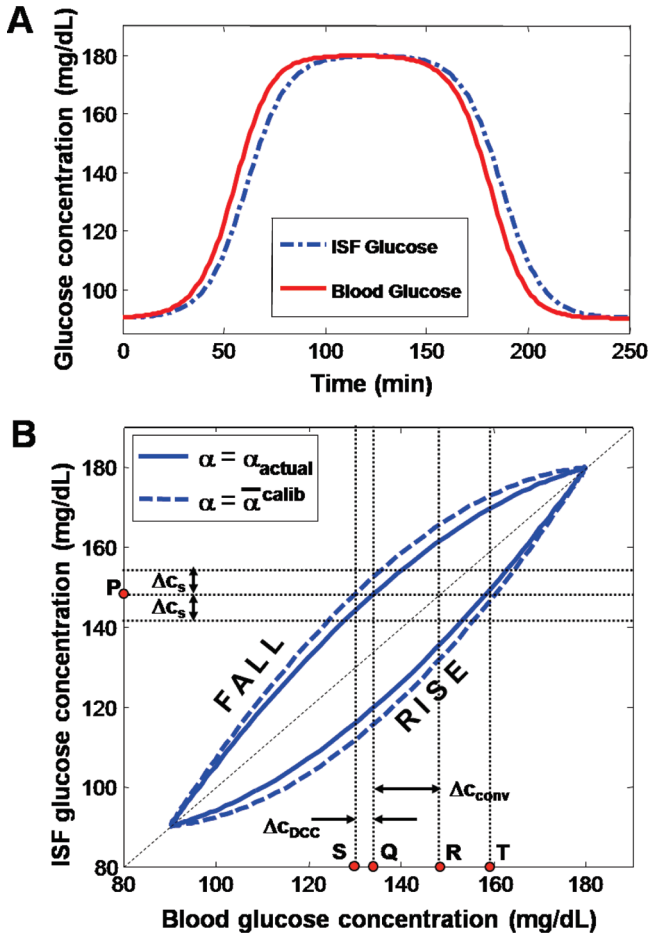

Figure 2. (A) Schematic representation of blood and ISF glucose concentration profiles, similar to those obtained during a typical tolerance test. (B) ISF vs blood glucose concentrations shown in panel A. The solid curve shows the lack of 1:1 correspondence between the actual ISF and blood glucose relationship, while the dotted curve represents the approximate relationship estimated by the DCC model. Further details are provided in the text.

However, the conventional models report the estimated ISF glucose concentration as the blood glucose concentration ($\hat{c}_{BG}$) in the prediction sample:

$$\hat{c}_{BG} = \hat{c}_{ISF} \tag{9}$$

Substituting eq 9 into eq 8 and rearranging, we obtain

$$\hat{c}_{BG} = c_{BG} - \alpha_{actual}\frac{dc_{ISF}}{dt} \pm \Delta c_s \tag{10}$$

Equation 10 implies that, under the conventional calibration framework, the limiting uncertainty in the concentration estimate has two separate contributions: (i) the uncertainty resulting from the measurement noise in the prediction spectrum and the spectral overlap, Δc_s, and (ii) the uncertainty due to the glucose physiological lag, $\Delta c_{conv} = \alpha_{actual}(dc_{ISF}/dt)$. While the former uncertainty (i) is a well-known quantity, the latter uncertainty (ii) has not been examined before. Figure 2 illustrates the two contributing factors of the prediction uncertainty. In this figure, the simulated blood and ISF glucose data in panel A (which mimics the glucose profiles obtained from a tolerance test) are plotted against each other to construct the solid curve in panel B. It is evident that the physiological lag between the blood and ISF glucose profiles in (A) introduces a hysteresis-like closed loop behavior when blood glucose is plotted against ISF glucose, showing the lack of a 1:1 correspondence between the glucose concentrations in the two compartments. For example, we observe that, given an ISF concentration of 148 mg/dL at point P, the actual blood glucose concentration could be either 132 mg/dL (Q) or 158 mg/dL (T). However, conventional methods that have the underlying assumption of a constant blood-to-ISF glucose gradient would predict 148 mg/dL (R), giving rise to a significant error in prediction. Specifically, when the glucose levels are increasing, the blood glucose concentrations are greater than the corresponding ISF glucose concentrations. This set of values is represented by the points on the concave upward curve (labeled "RISE"). Similarly, the set of values obtained during the falling phase is represented by the concave downward curve (labeled "FALL"). The lag uncertainty Δc_{conv} in the predicted blood glucose concentration for the conventional calibration model is given by the distance between points Q and R. The uncertainty due to the noise and spectral overlap in the prediction spectrum is marked as Δc_s.

Limiting Uncertainty for DCC Calibration. In contrast to the conventional model, the DCC scheme explicitly accounts for the physiological glucose dynamics. Specifically, the postprediction equation (PP-DCC) is used to transform the spectroscopy-based ISF glucose estimate ($\hat{c}_{ISF}$) to a corresponding blood glucose value ($\hat{c}_{BG}$), and this step needs to be considered in evaluating the limiting uncertainty. As the correct lag time constant in the prediction sample is unknown in a real clinical setting, some uncertainty due to the physiological lag is introduced via the PP-DCC step. As explained in the subsection "Limiting Uncertainty for Conventional Calibration", we employ the (ensemble) average of the lag time constants obtained from the calibration samples to approximate the actual lag time constant in the prediction sample. On the basis of this approximation, the PP-DCC equation can be rewritten as

$$\hat{c}_{BG} = \hat{c}_{ISF} + \bar{\alpha}^{calib}\frac{d\hat{c}_{ISF}}{dt} \tag{11}$$

where $\bar{\alpha}^{calib}$ refers to the average value of α computed from the calibration samples.

Substituting eq 7 into eq 11, we obtain

$$\hat{c}_{BG} = c_{ISF} \pm \Delta c_s + \bar{\alpha}^{calib}\frac{dc_{ISF}}{dt} \tag{12}$$

The deviation of $\bar{\alpha}^{calib}$ from the actual lag time constant in the prediction sample, α_{actual}, can be written as

$$\bar{\alpha}^{calib} = \alpha_{actual} \pm \Delta\alpha \tag{13}$$

where Δα is the error (uncertainty) in the estimation of the lag time constant.

Substituting eq 13 into eq 12 and rewriting the first term of the above equation as c_{BG}, we get

$$\hat{c}_{BG} = c_{BG} \pm \Delta\alpha\frac{dc_{ISF}}{dt} \pm \Delta c_s \tag{14}$$

Equation 14, which is analogous to eq 10 for the conventional calibration model, implies that, even with DCC, the net uncertainty is a combination of the uncertainties arising from the spectral noise and overlap (Δc_s) and the physiological lag ($\Delta c_{DCC} = \Delta\alpha(dc_{ISF}/dt)$). However, the primary difference between the two cases—with and without DCC—lies in the magnitude of uncertainty introduced due to the physiological lag. The lag uncertainty for the conventional calibration model case (which is proportional to α_{actual}) is significantly larger than that observed for DCC calibration (which is proportional to $\Delta\alpha$). This can be visualized in Figure 2B. The dashed curve of Figure 2B connects the points whose coordinates are given by the model *estimated* blood and ISF glucose concentrations (in contrast to the solid curve that represents the points whose coordinates are given by the blood and ISF glucose concentrations in Figure 2A). Since the exact lag time constant of the prediction sample is unknown, the estimated blood glucose concentrations will differ from the actual blood glucose concentrations by the product of the rate of change in the glucose concentration and the estimation uncertainty of the lag time ($\Delta c_{DCC} = \Delta\alpha(dc_{ISF}/dt)$). It is worth noting that the dashed (DCC-estimated) curve is computed using eq 11, whereas the blood and ISF glucose concentrations of the solid curve are related by eq 4. From the figure, it is evident that Δc_{DCC}, the distance between points Q and S, is substantially smaller than Δc_{conv}, the distance between points Q and R, as long as the lag time constant used in the DCC model provides a reasonably close approximation to the actual lag time constant. A quantitative comparison of the two lag uncertainties and the spectroscopic uncertainty is performed in the subsection "Experimental Studies on Human Subjects" in the Results and Discussion.

MATERIALS AND METHODS

We performed numerical simulations and experimental studies to (1) demonstrate the improvement in prospective prediction performance of the calibration model on application of DCC and (2) estimate the distribution of the lag time constant in a human population and characterize the prediction uncertainty introduced due to the physiological lag. To accomplish (1), a numerical simulation study was undertaken (next subsection). In this study, ISF and blood glucose concentration data sets, described by Steil et al.,[14,34] were used to generate tissue Raman spectra for calibration and prediction. The simulations were also used to understand the relationship between the SNR in the spectral data set and performance of the conventional and DCC calibration models. To investigate the lag time distribution in a human population (2), data sets obtained from our laboratory's clinical studies on human volunteers were employed. Additionally, the human volunteer study was used to determine the limiting uncertainty arising from the physiological glucose dynamics, as described in the second subsection in this section.

Numerical Simulations. The data set used in our numerical simulations was based on blood and ISF glucose concentrations originally measured by Steil et al.[34] In their studies, Steil and coworkers monitored blood and ISF glucose concentrations in nondiabetic human subjects during glucose clamping. After 10−12 h of overnight fasting, glucose was sequentially clamped at approximately 5, 4.2, and 3.1 mM (a 1 mM concentration of glucose ≈ 18 mg/dL) for 90 min each by insulin and glucose infusion and subsequently allowed to return to euglycemic levels. ISF glucose was measured by two MiniMed (Medtronic, Inc.) subcutaneous amperometric glucose sensors. Blood was withdrawn at regular intervals for blood glucose measurements using a clinical glucose analyzer. Our analysis uses the blood and ISF glucose concentrations from 90 to 380 min after initial insulin and glucose infusion, as shown in Figure 3. The simulated spectra and corresponding blood glucose concentrations are divided into calibration (data set spanning from 90 to 220 min) and prediction (data set from 230 to 380 min) sets, respectively.

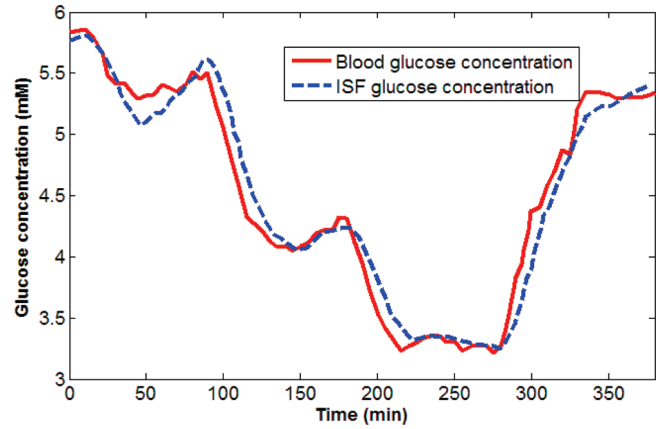

Figure 3. Blood and ISF glucose concentration−time profiles measured from a normal human volunteer during insulin-induced hypoglycemia.[34] Glucose was clamped at 5, 4.2, and 3.1 mM and subsequently allowed to return to normoglycemic levels. It is observed that the ISF glucose, measured by subcutaneous amperometric sensors, consistently lags blood glucose concentrations during both the rising and falling phases. In contrast, they have nearly identical values during the clamping phases. Reprinted from ref 34, Copyright 2005, with permission from Springer Science+Business Media: Diabetologia.

In our study, simulated Raman spectra are generated by forming weighted linear combinations of the constituent Raman spectra of glucose, creatinine, and urea (as measured by our laboratory Raman system[19]). The weights assigned for glucose (the analyte of interest) are determined by the experimentally measured ISF glucose concentrations of the Steil data set. The other two constituents (spectral interfering agents) are assigned weights that randomly varied within 2% of a constant value, to mimic the small changes observed in these constituents during typical glucose tolerance and clamping tests. To simulate normal experimental conditions, zero-mean Gaussian white noise is added to the mixture spectra at varying levels of SNR (20−40 dB) to study its effect on the prediction performance of the calibration models. The uniform noise across the spectra and the SNR range are consistent with those of typical Raman spectra of biological samples.

In contrast to the conventional PLS calibration strategy, where the number of loading vectors are optimized, in the DCC calibration the number of loading vectors and the lag time constant, α, need to be optimized. To accomplish this, we initially assign default values to α (0 min) and the number of loading vectors (2) employed, respectively. Prior to construction of the leave-one-out calibration model, all but one of the reference blood glucose concentrations are converted to the corresponding ISF

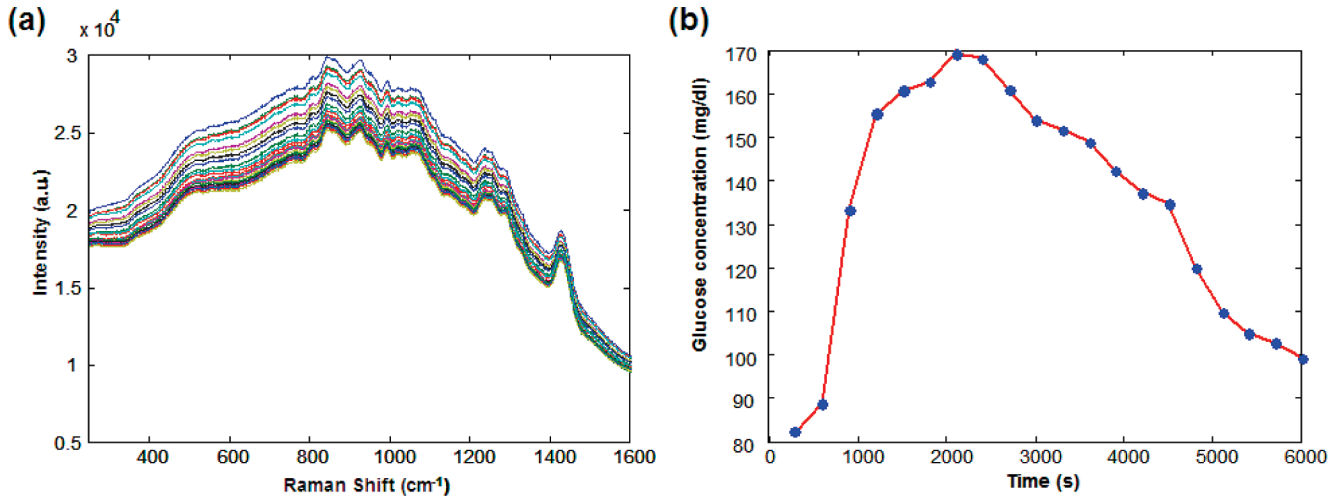

Figure 4. (a) Representative Raman spectra acquired from a human volunteer during OGTT. (b) Blood glucose concentration profile measured over the same time.

glucose values using PC-DCC (eq 5). This allows the creation of a calibration model based purely on ISF glucose. The developed calibration model, in conjunction with the spectrum of the excluded data point (which constitutes the validation data), is then used to predict the ISF glucose concentration at that point. Subsequently, PP-DCC (eq 4) is used to retransform the predicted ISF glucose concentration to the blood glucose value. This process is repeated until each data point is used once as the validation data. The resultant blood glucose estimates are compared with the actual blood glucose values to give the root-mean-squared error of cross-validation (RMSECV). The whole procedure is iterated for appropriate ranges of α (0−20 min) and number of loading vectors (LV) (2−10) to determine the optimal combination of parameters (α_{opt}, LV_{opt}) that yields the minimum RMSECV. This combination of parameters is then used to obtain the PLS regression vector, $\mathbf{b}_{opt}$. Prospective prediction on a separate portion of the data set was performed by taking the scalar product of the prediction spectra with $\mathbf{b}_{opt}$ (eq 2). The ISF glucose predictions are reconverted to the blood glucose values using PP-DCC, where α_{opt} is used in place of α in eq 4. The root-mean-squared error of prediction (RMSEP) is computed from the predicted blood glucose concentrations and the reference blood glucose values.

Conventional PLS calibration and prediction is also performed on the same data set to compare the relative performance with that of the DCC model. For further comparison, a fixed time delay is also incorporated into the standard PLS analysis as a second control. This involves shifting the measured blood glucose concentrations with respect to the spectral acquisitions by a specified amount comparable to the time lag reported in the literature. Twenty simulations are carried out for each value of SNR in the spectral data set (both calibration and prediction) to establish the mean and standard deviation of the prospective prediction errors.

Experimental Studies on Human Subjects. To investigate the lag time distribution in a human population, clinical data sets consisting of blood glucose concentrations and tissue Raman spectra are used. The acquisition of the clinical data was described in one of our laboratory's previous papers.[11] Briefly, Raman spectra were collected from the forearms of healthy Caucasian and Asian human volunteers undergoing OGTT. The age of the tested human volunteers was in the range of 21−29, with a mean of 24.5. For the excitation source, an 830 nm diode laser (Process Instruments) was used at an average power of ∼300 mW in a ∼1 mm^2 spot. An f/1.8 spectrograph (Kaiser Optical Systems) was coupled to a liquid nitrogen-cooled CCD (1340 × 1300 pixels, Roper Scientific) for spectral dispersion and acquisition, respectively. For each volunteer, OGTT was initiated by the ingestion of a glucose-rich solution, and Raman spectra were collected every 5 min over a 2 h period. Concurrently, the reference blood glucose concentrations were measured every 10 min from blood samples using a clinical glucose analyzer (HemoCue, Inc.), and spline interpolation was used to correlate the measured blood glucose concentrations with the spectra collected at intermediate time points. This study protocol was approved by the MIT Committee on the Use of Humans as Experimental Subjects.

Data sets from volunteers exhibiting motional artifacts, inadequate SNR in the acquired spectra, and impaired glucose tolerance characteristics are excluded from further analysis. A representative set of tissue Raman spectra and the corresponding blood glucose concentration profile acquired from one of the human volunteers are shown in Figure 4. For the selected volunteer data sets, DCC calibration is performed using a leave-one-out cross-validation routine on the measured Raman spectra and reference blood glucose concentrations to determine the optimal value of α for each individual. In addition, conventional PLS calibration is also performed on the same data sets to compare the resultant cross-validation errors. The cross-validation procedures in both cases remain the same as that described in the previous subsection, except that experimentally measured Raman spectra are used in place of the simulated Raman spectra. The mean and standard deviation of α determined from the human subjects are used to approximate α_{actual} and Δα for the quantification of uncertainty due to physiological lag for the DCC and conventional calibration schemes, respectively (section "Formulation of Prediction Uncertainty Arising from Physiological Lag"). These uncertainty estimates are also compared with the spectroscopic uncertainty, Δc_s.

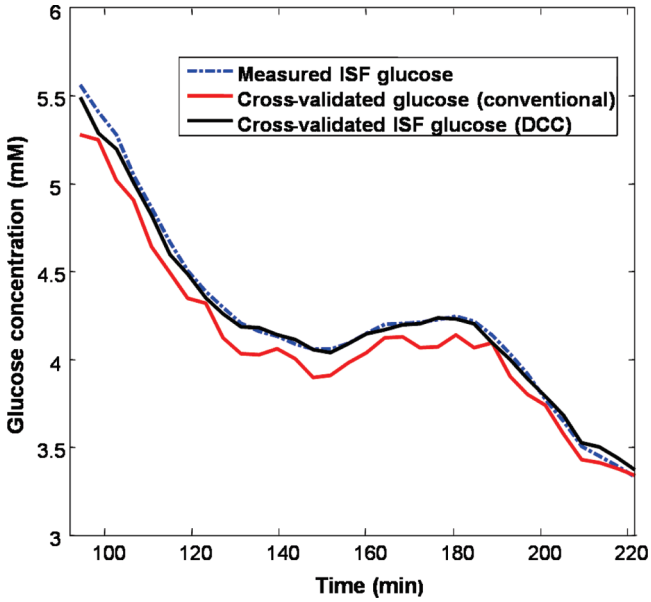

Figure 5. Cross-validation results of conventional (red) and DCC (black) calibration methods applied to the simulated data set. The measured ISF glucose concentration values are given by the blue dotted line. In the DCC calibration process, the lag time constant, α_{opt}, was optimized to be 6.1.

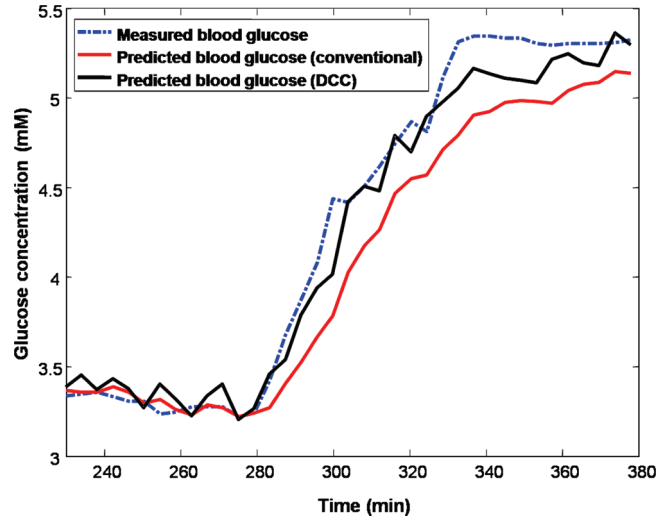

Figure 6. Prospective prediction results of conventional (red) and DCC-based (black) calibration methods applied to the simulated data set. The measured blood glucose concentration values are given by the blue dotted line.

RESULTS AND DISCUSSION

Numerical Simulations. Numerical simulations were used to compare the prospective prediction capability of the conventional and DCC calibration models. DCC implementation was found to reduce the RMSECV of the simulated data set from 0.15 to 0.04 mM, when the measured ISF glucose concentrations were used for computing the cross-validation errors. The RMSECV for fixed timed delay PLS processing was computed to be 0.07 mM. These simulation results were obtained for an SNR of 40 dB. Figure 5 shows the measured ISF glucose concentrations plotted together with cross-validated glucose concentrations from the conventional and DCC calibration models. It is evident that the ISF glucose concentration profile generated with DCC closely matches the measured ISF glucose concentrations, while that generated without DCC shows significantly larger deviations. The cross-validation routine also optimized the lag time constant for the DCC calibration model and the number of loading vectors for both models. For this data set, the characteristic lag time constant, α_{opt}, was determined to be 6.1 min, in agreement with the experimentally observed values of 6−8 min.[34]

When the calibration models were applied prospectively to the prediction data set, the DCC model (RMSEP = 0.14 mM) exhibited significantly improved prediction accuracy compared with the conventional PLS scheme (RMSEP = 0.28 mM). In comparison, the fixed time delay PLS processing provides an RMSEP of 0.26 mM, which is a slight improvement over conventional PLS implementation, but it is still significantly poorer than the DCC performance. Figure 6 shows the results of prospective prediction, in which the measured blood glucose concentration profile is plotted alongside the prediction profiles, with and without DCC. This demonstrates how calibration during nonequilibrium conditions leads to systematic errors, giving rise to much higher prediction errors (Figure 6) than estimated during cross-validation (Figure 5). The presence of systematic errors is further evidenced by the relative performance of the fixed time delay processing in cross-validation (approximately 50% improvement over conventional PLS processing) and prospective prediction (approximately 7% improvement over conventional PLS processing). In fact, in the presence of such errors, the predicted glucose concentration may have no statistically significant correlation with the actual glucose concentrations during rapidly rising and declining glucose concentrations. Potentially, one could achieve an even closer correlation with the measured blood glucose concentration profile by smoothing out the noisy fluctuations observed in the concentration profile of the DCC prediction of Figure 6. However, such smoothing algorithms were not employed as they might introduce artifacts and additional delays to the concentration profile that are unrelated to glucose equilibration.[34]

The accuracy of blood glucose concentration prediction with and without DCC was also compared at varying levels of SNR in the spectral data set. Figure 7 shows a plot of the RMSEP of blood glucose prediction with conventional and DCC calibration models as a function of SNR. In both cases, an increase in noise level corresponded to an increase in error values, as expected. However, under all tested values of SNR, the prediction error of DCC calibration models was consistently smaller compared to that of the conventional PLS models. It was also observed that the mean α_{opt} was essentially noise-insensitive, although the variations from the mean α_{opt} were larger for lower SNR (e.g., the standard deviation in α was computed to be 0.05 and 0.5 min at 40 and 20 dB, respectively).

Clearly for DCC implementation, a time series of glucose measurements (such as those obtained from glucose tolerance tests) are required from human subjects included in the calibration study for characterization of the glucose kinetics. It is not possible to develop a consistent calibration model based only on single spectroscopic measurements from multiple human subjects, as such measurements do not provide information on the glucose kinetics.

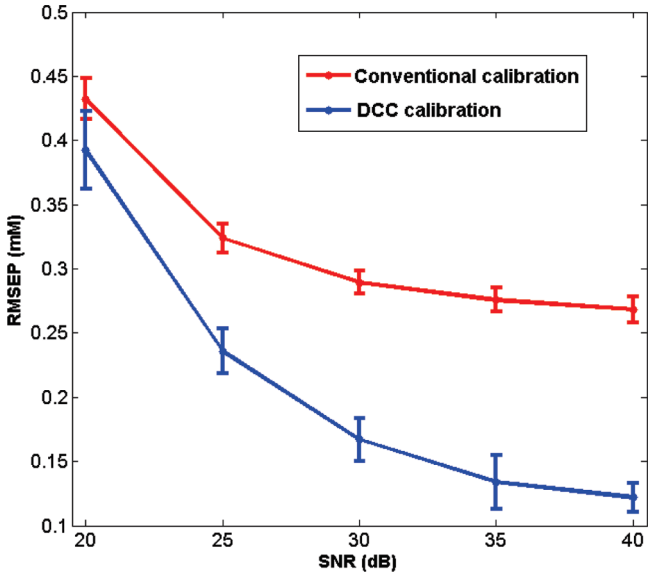

Figure 7. RMSEP obtained for conventional (red) and DCC (blue) calibration models, applied to the simulated data set, as a function of increasing SNR. The error bars represent the standard deviation of RMSEP for 20 iterations.

Table 1. Summary of Cross-Validation Results of Conventional and DCC Calibration Models Applied to the Human Volunteer Data[a]

		DCC model		conventional model	
volunteer	no. of data points	α_{opt} (min)	RMSECV (mM)	RMSECV (mM)	change in RMSECV (%)
1	25	9.5	0.87	1.07	19.10
2	26	11.5	0.52	0.72	27.56
3	26	10.5	0.70	0.97	28.62
4	30	11.1	1.02	1.08	5.74
5	25	8.4	0.68	0.79	13.35
6	26	8.4	0.64	0.82	22.00
7	25	7.5	0.42	0.51	17.61
8	29	8.1	0.76	0.87	12.44
9	31	8.3	0.96	1.00	3.41
10	27	12	0.50	0.53	5.25

[a] See the subsection "Experimental Studies on Human Subjects" in the Materials and Methods.

It is also worth noting that application of an enhanced calibration scheme, such as support vector machines[39] or hybrid calibration methods,[40,41] alone would not alleviate inconsistencies in the calibration models as they do not address the lack of 1:1 correspondence between the ISF and blood glucose concentrations (Figure 2). Nevertheless, when used in conjunction with DCC, such calibration schemes may potentially further improve the prediction accuracy.

Experimental Studies on Human Subjects. Table 1 lists the results of the leave-one-out cross-validation on the data set from each human subject, using DCC calibration as well as the conventional PLS routine. We observe that, on average, the RMSECV for the blood glucose concentrations of the human subjects decreases on application of DCC by 15.5%, with a maximum decrease of 28.6%. This demonstrates the applicability of DCC in clinical situations, where the number of tissue components probed is vastly greater than the three constituents (glucose, creatinine, and urea) employed in our simulations.

As mentioned in the section "Dynamic Concentration Correction Theory", in formulating DCC, it has been assumed that the sampling volume is a subset of the interstitial fluid space. This assumption was based on the facts that (i) NIR light has a penetration depth of ~1 mm in skin tissue and (ii) the blood vessels contribute only 5% to the total skin volume,[36] with the outermost epidermis being completely avascular. However, a small fraction of the inelastically scattered (Raman) light arises from the glucose residing in the blood compartment. This results in a reduction in the value of the lag time constant, α, as determined by our DCC model. Nevertheless, our results demonstrate that DCC successfully models the clinical human volunteer data, even though a small Raman contribution from the blood glucose component is present. This shows that the DCC approach is effective in improving consistency in the calibration model and thus in prospective prediction, as long as the spectral contribution of blood glucose is small compared to that of ISF glucose.

The results also suggest that the value of the lag time is fairly constant for the tested human volunteer population. This is established by the lag time distribution obtained from the clinical data, where the mean of α, 9.5 min, is significantly larger than the standard deviation, 1.6 min. The relative constancy of α indicates that the mean lag time of the calibration set provides a fairly accurate approximation to the lag time of any prospective subject on whom the algorithm has not been applied before. To the best of our knowledge, this is the first time that the lag time distribution in a human population has been measured by optical techniques. Previous attempts with subcutaneous amperometric sensors have been observed to have significant sensor-specific lag, which obscures the precision of the physiological lag measurements.[14] In addition to the sensor-specific lag of the subcutaneous amperometric monitors, the difference in lag time constants observed from the numerical simulations using the Steil data set (6.1 min) and our clinical studies on human volunteers (9.5 ± 1.6 min) can be attributed to (a) the difference in the composition of glucose (i.e., the proportion of blood and ISF) sampled by the spectroscopic and amperometric sensors and (b) the variations in the population demographics studied in the two cases.

Although most current research including our own study on human subjects reported above indicates a reasonably constant value of α, some research groups have previously suggested that the response times between blood and ISF glucose may be different for the rising and falling phases. These groups claim to have demonstrated that ISF glucose falls in advance of blood glucose during the time of declining glucose levels.[42−44] In such situations, a modified DCC model can be implemented by

(39) Thissen, U.; Ustun, B.; Melssen, W. J.; Buydens, L. M. C. *Anal. Chem.* **2004**, *76*, 3099–3105.
(40) Berger, A. J.; Koo, T. W.; Itzkan, I.; Feld, M. S. *Anal. Chem.* **1998**, *70*, 623–627.
(41) Shih, W.-C.; Bechtel, K. L.; Feld, M. S. *Anal. Chem.* **2007**, *79*, 234–239.
(42) Sternberg, F.; Meyerhoff, C.; Mennel, F. J.; Mayer, H.; Bischof, F.; Pfeiffer, E. F. *Diabetologia* **1996**, *39*, 609–612.
(43) Aussedat, B.; Thome-Duret, V.; Reach, G.; Lemmonier, F.; Klein, J. C.; Hu, Y.; Wilson, G. S. *Biosens. Bioelectron.* **1997**, *12*, 1061–1071.
(44) Thome-Duret, V.; Reach, G.; Gangnerau, M. N.; Lemonnier, F.; Klein, J. C.; Zhang, Y.; Hu, Y.; Wilson, G. S. *Anal. Chem.* **1996**, *68*, 3822–3826.

employing two distinct α values during the rising and falling phases through a piecewise application of eqs 4 and 5.

The mean and standard deviation of α obtained on the human volunteer data set were also employed in determining the physiological lag uncertainties for the DCC and conventional calibration schemes. For the conventional schemes, the uncertainty is calculated as $\alpha_{actual}(dc_{ISF}/dt)$, where the mean α of the human volunteers is used for α_{actual}. At times of reasonably rapid increase in glucose levels, the concentration of glucose in either compartment may change by ~2 mg/dL/min (0.11 mM/min).[15] Plugging in these values, we find that, for conventional calibration, the prediction uncertainty due to lag amounts to approximately 1.06 mM. For the DCC model, the uncertainty due to lag can be computed by $\Delta\alpha(dc_{ISF}/dt)$, where Δα is approximated by the standard deviation of α obtained from the human volunteer data set. On the basis of this value of Δα, we obtain a lag uncertainty of 0.18 mM for the DCC calibration method. The calculated values project to an approximately 6-fold reduction in the lag uncertainty on application of DCC.

Previously, we had estimated using tissue phantom studies that the spectroscopic uncertainty for glucose using our Raman instrument was 1.04 mM (obtained for $\sigma = 61.03$ (photon counts), $s_g = 83.74$ (photon counts/mM), and $olf_g = 1.43$ in eq 6b).[19] Prior to this work, this spectroscopic uncertainty was considered to be the limit of detection, i.e., the smallest concentration at which glucose could be detected in the tissue. For the specific case of noninvasive glucose detection, this does not provide the full picture, as it ignores the lag uncertainty. For example, when conventional calibration schemes are employed, our results suggest that the uncertainty due to lag (1.06 mM) is comparable to the spectroscopic uncertainty (1.04 mM), especially at times of rapid changes in glucose levels. Consequently, the resultant limit of detection, which is the sum of the uncertainties arising from spectroscopic considerations and physiological lag (2.1 mM), may be nearly twice that of the previously accepted value (1.04 mM). On the other hand, the net uncertainty on application of DCC (1.22 mM) predominantly arises from spectroscopic considerations (SNR and spectral overlap), and the glucose kinetics plays only a minor role.

CONCLUSION

The presence of a physiological lag between glucose in the blood and ISF compartments must be considered in developing an accurate spectroscopy-based calibration model for predicting blood glucose concentrations. We have presented a mass transfer model based correction scheme that explicitly accounts for the glucose kinetics. The proposed DCC enables us to employ the reference concentrations that are appropriate for the acquired spectra in developing the calibration model—a key step which has not been previously considered. In particular, the resulting improvement in blood glucose estimates should enhance the spectroscopic ability to correctly determine hypoglycemia and even predict impending hypoglycemia on the basis of the rate of change in glucose concentration. Furthermore, we have demonstrated that the prediction uncertainty due to physiological lag, which is comparable in magnitude to the uncertainty arising from noise and nonorthogonality in the spectral data set, can be reduced substantially by employing DCC.

We are currently performing a clinical study to characterize the glucose kinetics in a larger population of human subjects of different ages and ethnicities, both with and without diabetes. It is well-known that inadequate glycemic control causes microvascular and macrovascular changes,[45] which may in turn affect the physiological lag time. We expect that this study will provide further details about such changes and the ability of spectroscopy to diagnose similar diabetes-related complications. In addition, the clinical study across a larger and more diverse population would lead to a better understanding of the applicability of the DCC model as well as the variation of the lag time across different population segments. This clinical study is also expected to shed light on tissue site selection for spectroscopic sensing on the basis of a combination of skin heterogeneity and glucose kinetics parameters. In addition, our future research will focus on combining DCC with nonlinear and hybrid regression schemes to develop more robust and accurate calibration models.

ACKNOWLEDGMENT

This research was supported by the NIH National Center for Research Resources (Grant P41-RR02594) and a grant from Bayer Health Care. I.B. was supported by the Lester Wolfe fellowship. The first two authors contributed equally to this work.

APPENDIX I

A first-order accurate estimate of the blood glucose concentration can be obtained by using a finite difference approximation for the derivative term of eq 4:

$$c_{BG}(t) = c_{ISF}(t) + \alpha\frac{c_{ISF}(t) - c_{ISF}(t - \Delta t)}{\Delta t} \qquad (15)$$

where Δt is the time interval at which spectroscopic measurements (and, thus, ISF glucose concentration estimates) are obtained. The above equation gives the discrete transformation equation of the postprediction (PP-DCC) step, which can be applied in real time. There are a couple of points worth noting about the application of eq 15. First, it is evident from the above equation that at least two spectroscopic predictions of ISF glucose (at t and $t - \Delta t$) are necessary to determine the blood glucose concentration at time t. In practice, it is beneficial to perform multiple spectroscopic acquisitions so that the corresponding blood glucose estimates can be averaged to ensure less fluctuations in the predicted blood glucose value. Second, the time interval, Δt, at which the spectroscopy-based ISF glucose predictions should be performed, needs to be ascertained. Although spectroscopic acquisitions can be performed rapidly, having a very small Δt is not too useful as it may fail to capture the changes in the glucose levels due to the slow diffusion kinetics—thereby rendering the DCC approach ineffective. On the other hand, too large a time interval would introduce substantial errors in the derivative term. Using these limiting cases as guidelines, one might optimize the value of Δt with a starting point given by a fraction of the typical physiological lag time (~5−10 min).

APPENDIX II

After integration by parts was employed for the second term of eq 5, numerical integration was performed by using Simpson's rule to get the following equation:

$$c_{ISF}(t_f) = c_{BG}(t_f) + (c_{ISF}(t_i) - c_{BG}(t_i)) \times \exp\left(-\frac{t_f - t_i}{\alpha}\right) - \frac{t_f - t_i}{6}A \quad (16a)$$

where

$$A = \dot{c}_{BG}(t_i)\exp\left(-\frac{t_f - t_i}{\alpha}\right) + 4\dot{c}_{BG}\left(\frac{t_i + t_f}{2}\right) \times \exp\left(-\frac{t_f - t_i}{2\alpha}\right) + \dot{c}_{BG}(t_f) \quad (16b)$$

Here, $\dot{c}_{BG}(t)$ refers to the derivative of c_{BG} evaluated at t. This equation can be readily evaluated by approximating $\dot{c}_{BG}(t)$ via a first-order finite difference approximation similar to that employed in eq 15 for the PP-DCC step (Appendix I). The resultant discretized version of eq 16a gives the necessary transformation equation for the PC-DCC step. The primary challenge in the evaluation of this equation lies in having a priori knowledge of the initial ISF glucose value, i.e., at the start of the time window $[t_i, t_f]$. Generally, such information is not available for an arbitrary time window. However, during a spectroscopic calibration study such as glucose clamp or tolerance test, one can ensure that the ISF glucose and blood glucose values are completely in equilibrium at the start of the experiment by restricting the glucose intake of the subject prior to the measurements. For example, a typical oral glucose tolerance test (OGTT) protocol stipulates that the patient must fast for 8−14 h before the study.[46] This initial condition enables successful evaluation of eq 16b for the first time window. For each subsequent evaluation, the ISF glucose value at time t_f for the previous window is input as the initial value (at time t_i) for the current window. Evidently, the shorter the time window over which the evaluation is performed, the higher the accuracy of the determined ISF glucose concentrations. Nevertheless, the time window cannot be shortened below a lower bound, governed by the maximum permissible frequency of blood withdrawal from a human subject. Most research laboratories, for example, sample blood glucose at time intervals ranging from 2.5 to 10 min.[14,34,47] To determine the values of the concentrations and their derivatives at intermediate points, spline interpolation is employed.

(45) Reusch, J. E. B. *J. Clin. Invest.* **2003**, *112*, 986–988.
(46) American Diabetes Association. *Diabetes Care* **2009**, *32*, S13−S61.
(47) Maruo, K.; Oota, T.; Tsurugi, M.; Nakagawa, T.; Arimoto, H.; Tamura, M.; OzakiI, Y.; Yamada, Y. *Appl. Spectrosc.* **2006**, *60*, 441–449.

Received for review March 29, 2010. Accepted June 12, 2010.

AC100810E